2011

Lead-Acid Battery Model Under Discharge with a Fast Splitting Method

R. Corban Harwood
George Fox University, rharwood@georgefox.edu

Valipuram S. Manoranjan

Dean B. Edwards

Lead-Acid Battery Model Under Discharge With a Fast Splitting Method

Richard Corban Harwood, Valipuram S. Manoranjan, and Dean B. Edwards

***Abstract*—A mathematical model of a valve-regulated lead-acid battery under discharge is presented as simplified from a standard electrodynamics model. This nonlinear reaction–diffusion model of a battery cell is solved using an operator splitting method to quickly and accurately simulate sulfuric acid concentration. This splitting method incorporates one-sided approximation schemes to preserve continuity over material interfaces encompassing discontinuous parameters. Numerical results are compared with measured data by calculating battery voltage from modeled acid concentration as derived from the Nernst equation.**

***Index Terms*—Batteries, discharge, lead, modeling, nonlinear systems, splitting.**

NOMENCLATURE

A_j	Electrode cross-sectional area in region $j = 1, 3$.
A_j^S	Electrode active surface area per volume in region $j = 1, 3$.
b_j	Simplifying reaction constant in region $j = 1, 2, 3$.
c	Concentration of sulfuric acid.
c^0	Initial sulfuric acid concentration.
D	Reference diffusion rate.
F	Faraday's constant: $F = 96,487$ c/mol.
f	Mean molar activity coefficient for H_2SO_4.
i	Cell-pair current density.
i^{app}	Cell-pair discharge current density.
i_j^0	Exchange current density in electrode $j = 1, 3$.
K_j	Equivalent molarity to charge constant in electrode $j = 1, 3$.
L_j	Thickness of region $j = 1, 2, 3$.
R	Universal gas constant: $R = 8.3145$ J/(mol·K).
r	Bulk cell resistance.
t^+	Transference number for H^+ ions.
u	Electrode utilization.
u_j^{CVF}	Critical volume fraction in electrode $j = 1, 3$.
V	Battery voltage.
W_j	Weight of active material in electrode $j = 1, 3$.
α_j	Anodic transfer coefficient in electrode $j = 1, 3$.
ε_j	Porosity: acid-filled volume fraction of region $j = 1, 2, 3$.
κ_j	Charge density for electrode $j = 1, 3$.
η_j	Surface overpotential of electrode $j = 1, 3$.

I. INTRODUCTION

DEMAND for advancing vehicular technology has increased in recent years. There is a great need for better and cheaper hybrid electric automobiles. Many factors have added to this growing need, including the high costs of petroleum, the volatile nature of its market, and the fear of its depleting sources, as well as global concern over carbon emissions. Over a ten year span from January 2000 to January 2010, U.S. crude oil costs quadrupled, including a one-year doubling from 2007 to 2008 [1]. While demand held steady over this decade [2], oil production faltered midway, decreasing for the first two consecutive years in 2006 and 2007 [3]. Political and individual concerns over carbon emissions have greatly increased in recent years, because of health risks as well as current and future damage to the environment. Due to the combination of these factors and the anticipated benefits of alternate fuels, the need for research and development of alternate energy sources, specifically for personal transportation, is critical in manufacturing hybrid/electric vehicles.

Such research is being done, for example, at University of Idaho's Center for Intelligent Systems Research (CISR), where valve-regulated lead-acid (VRLA) batteries are being designed and developed for optimal energy-to-weight ratios as an integral part of a complete electric vehicle system [4]–[8].

This paper presents a model and numerical method for simulating sulfuric acid as well as voltage dynamics in a VRLA battery.

A. Previous Research

Early mathematical models developed to describe lead-acid batteries date back to 1958 with Stein [9] and 1961 with Euler [10], and focused on the positive electrode dynamics only. Newman and Tiedemann [11] provide a summary on the numerous contributions that improved these early models. Gu *et al.* [12] in 1987, followed by Salameh *et al.* in 1991 [13], further expanded these improvements into a mathematical model describing the dynamics of the five major electrochemical components during a full cycle of discharge, charge, and rest for a complete battery cell pair: acid concentration, electrode porosity, electrolyte current density, electrode potential, and

electrolyte (liquid) potential. Temperature and several other variables were assumed constant.

This basic model was expanded in 2001 by Tenno *et al.* [14] by reevaluating some of the underlying model equations. The calculated voltage of this expanded model was remarkably accurate, yet the voltage modeled used was not clearly specified. The traditional model continues to be adapted, with contributions focusing more recently on voltage restorers [15], the VRLA reference electrode [16], and parameter estimation [17].

Separately, a model for acid concentration exclusively based upon conservation of mass and reactive electrode surface was developed by Appel [4], [18], Gill [19], and Cantrell [20] starting in 1987. These models focused on compartmentalizing physical and chemical components. Their separate treatment of reaction and diffusion processes inspired us to apply an operator splitting method. As influenced by the compartmental focus of their model, we augmented our dynamical system with stopping criterion for concentration, voltage, and utilization thresholds. The latter threshold, supported by work in 3-D conductivity models [21], [22] led to a novel calibration technique relating severe voltage variation to incomplete formation of charge.

This paper's contributions are as follows.

1) We construct a reaction–diffusion model exclusively for the concentration of sulfuric acid in a VRLA battery through relevant simplifying assumptions to the model adapted by Tenno *et al.* [14]. This new simplified model is analyzed and validated by experimental data.
2) We develop an operator splitting numerical method to split the given nonlinear partial differential equation (PDE) into an analytically solvable reaction step and a linear diffusion step. Our results show that this splitting runs considerably faster than the "real time" cited by Tenno *et al.* [14], while maintaining consistency and stability. Further, in comparison to a full method, where the operator is not split, our split method performs with superlinear speedup.
3) We develop numerical schemes to preserve the first order in time and second order in space accuracy over the discontinuous interfaces. The interval centering discretizations of the regions avoids material interfaces where parameter values cannot be determined.
4) We calculate battery voltage from our sulfuric acid concentration using a model derived from the Nernst equation [23] and inverting the Butler–Volmer equation [14] through a bounded line search optimization, and then we compare this calculated voltage to measured data from 1-h rate discharge tests of similarly manufactured batteries. Due to the high variability in the data, we propose a calibration of reducing the initial fullness of charge to better simulate the voltage.

The general diffusion model is developed for the acid concentration in Section II along with descriptions and justifications for assumptions leading to our simplified model. This is followed by construction of the battery voltage model based on this concentration. In Section III, the numerical operator splitting method is described and analyzed for accuracy and stability. Section IV presents the results of the numerical simulations for concentration and voltage as well as a list of parameter values used. The simulated voltage is contrasted with a batch of measured data and then the further calibrated voltage is compared against three representative data samples. These results are then discussed in Section V.

II. Development of Reaction–Diffusion Model

In general, a VRLA battery is a combination of battery cells, where each cell is composed of a stack of alternating negative and positive electrodes, separated by a highly porous sheath called the separator, and saturated with sulfuric acid. A pressure sensitive release valve accompanies the outer casing to manage the gases created by the normal reactions. A cell pair consists of half of a negative electrode, one separator layer, and half of a positive electrode, where middles of each electrode at the outer boundaries of the cell pair mark the current collecting grids [5].

A. Simplifying Assumptions

To simplify and combine the expanded model [14] into an initial boundary value problem, we assume that discharge current, temperature, active surface area, and porosity are constants, using averaged values where appropriate, and that overpotential is assumed constant at each step, and then updated. The following is the justification for these simplifying assumptions.

The batteries tested are discharged at constant currents and kept in a controlled temperature setting, validating our assumptions of constant current and temperature. Since the batteries we model were newly formed when tested, and due to the rechargeable nature of the lead-acid battery, we assume that the capacity does not drop appreciably between the first few charge–discharge cycles. Tenno *et al.* argue that active surface area is relatively constant if "small variation of battery capacity is considered" [14], so we utilize their assumption for the active surface area. Overpotential is statically updated as an averaged value in each region to represent equally distributed current over the remaining nodes. As the battery current is held constant and overpotential is defined by the generated current in each node, this averaged value should remain constant until nodes become fully discharged. Finally, changing porosity from a dynamic to a static variable considerably simplifies the model from a coupled nonlinear system of two PDEs to one nonlinear PDE. Thus, an average value will be used as an approximation.

Under certain tolerances, each component of the battery is manufactured uniformly, particularly the paste on the preformed electrodes. This means that any cross section of the battery cell cut perpendicular to the electrodes yields the same material properties, and, thus, the same electrochemical dynamics. Also, each individual cell pair is mirrored throughout each battery cell. By these symmetries, we reduce the 3-D problem down to a perpendicular line through an individual cell pair with end points at the lead grids at the centers of the negative and positive electrodes, respectively. Because of the discontinuities of the material properties within this spatial region $(0, L)$, we decompose it into three disjoint regions, $(0, L_1)$, (L_1, L_2), and (L_2, L), corresponding to the negative electrode half, separator, and the positive electrode half, respectively,

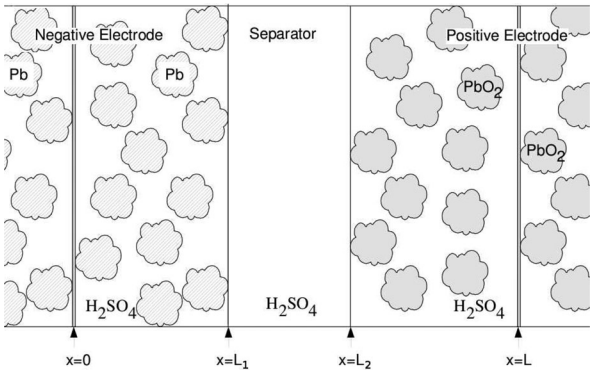

Fig. 1. 2-D representation of a fully charged battery cell pair.

as shown in Fig. 1. Thus, our PDE is computed in the space $(x,t) \in (0,L_1) \cup (L_1,L_2) \cup (L_2,L) \times (0,\infty)$. It is reasonable to assume that acid concentration is a continuous function, since this fluid flows throughout the composite material. To preserve this continuity of solution, we apply matching flux conditions at the interfaces of the material regions [12]. Combining the governing PDE over the domain $[0,L]$ with outer and inner boundary conditions and an initial condition of uniform distribution (to simulate the battery starting at rest), we have the initial boundary valued problem over $[0,L] \times [0,\infty)$ as described by the following three coupled subproblems.

B. Concentration Model

We develop our model by applying the previous simplifying assumptions to the following reaction–diffusion model for acid concentration [14]

$$\varepsilon \frac{\partial c}{\partial t} = \frac{\partial}{\partial x} D\varepsilon^{\beta} \frac{\partial c}{\partial x} + (cK_1 + K_4)\frac{\partial i}{\partial x}$$
$$\text{with } c(x,0) = c_{\text{ref}}, \qquad t > 0$$

with additional relations

$$K_1 \frac{\partial i}{\partial x} = \frac{\partial \varepsilon}{\partial t}$$
$$\frac{\partial i}{\partial x} = \mathcal{A} i_0 \left(\frac{c}{c_{\text{ref}}}\right)^{\beta} \cdot \left(\exp\left\{\frac{\alpha_a F \eta}{RT}\right\} - \exp\left\{\frac{(\alpha_a - 2)F\eta}{RT}\right\}\right)$$

where ε is the porosity, c and c_{ref} are the variable and initial sulfuric acid concentrations, D is the diffusion coefficient, β is the tortuosity exponent, K_1 is the volume-to-charge ratio, K_4 is the molarity to charge ratio, i is the current density, α_a is the anodic apparent transfer coefficient, $\mathcal{A}$ is the active surface area per volume, i_0 is the exchange current density, F is Faraday's constant, η is the overpotential, R is the universal gas constant, and T is the temperature. For simplification, we write $K \equiv K_4$, $i^0 \equiv i_0$, $\alpha \equiv \alpha_a$, $A^S \equiv \mathcal{A}$, and approximate $\beta = 0.5$ to match the morphology of the twistedness of the path for discharge [14]. To simplify and combine the expanded model [14] into an initial boundary value problem, we assume that discharge current, temperature, active surface area, overpotential, and porosity are constants. Consequently, $\frac{\partial \varepsilon}{\partial t} = 0$, so we drop the K_1 portion of the reaction term.

Symmetry and continuity of the concentration are preserved at the current-collecting grid in the center of the negative electrode

$$\frac{\partial c}{\partial x}(0,t) = 0, \;\; t > 0. \tag{1}$$

In the relevant half of the negative electrode, charge is released during discharge as the lead (Pb) and sulfuric acid (H_2SO_4) react, diminishing the concentration, to produce lead sulfate ($PbSO_4$) and release hydrogen gas (H_2) [5]. This consumption and diffusion of sulfuric acid are modeled by the reaction–diffusion equation

$$\frac{\partial c}{\partial t} = \frac{D}{\sqrt{\varepsilon_1}} \frac{\partial^2 c}{\partial x^2} - b_1 \sqrt{c} \tag{2}$$
$$\text{with } c(x,0) = c^0, \qquad 0 < x < L_1, \; t > 0.$$

At the interface between the negative electrode and separator, the material and chemical parameters change abruptly. To preserve fluidity, the continuity of the concentration is preserved and the flux across the interface is matched by the equations

$$c(L_1^-,t) = c(L_1^+,t) \tag{3}$$
$$D\sqrt{\varepsilon_1}\frac{\partial c}{\partial x}(L_1^-,t) = D\sqrt{\varepsilon_2}\frac{\partial c}{\partial x}(L_1^+,t) \tag{4}$$
$$\text{where } L_j^- = \lim_{x \to L_j^-} x, \qquad L_j^+ = \lim_{x \to L_j^+} x, \;\; t > 0.$$

Since the material composing the separator mesh is inert with respect to the sulfuric acid, concentration is merely diminished by the fluidic diffusion outward to the two electrodes, as described by the diffusion equation

$$\frac{\partial c}{\partial t} = \frac{D}{\sqrt{\varepsilon_2}} \frac{\partial^2 c}{\partial x^2} \tag{5}$$
$$\text{with } c(x,0) = c_{\text{ref}}, \qquad L_1 < x < L_2, \; t > 0.$$

At the separator–positive electrode interface, the discontinuity of the material parameters is similarly countered by preserving concentration continuity and matching the flux to preserve fluidity

$$c(L_2^-,t) = c(L_2^+,t), \;\; t > 0 \tag{6}$$
$$D\sqrt{\varepsilon_2}\frac{\partial c}{\partial x}(L_2^-,t) = D\sqrt{\varepsilon_3}\frac{\partial c}{\partial x}(L_2^+,t), \;\; t > 0. \tag{7}$$

In the positive electrode half, charge is absorbed during discharge as the lead dioxide (PbO_2) and sulfuric acid react, again diminishing the concentration, to produce lead sulfate and water (H_2O) [5]. This is modeled by

$$\frac{\partial c}{\partial t} = \frac{D}{\sqrt{\varepsilon_3}} \frac{\partial^2 c}{\partial x^2} - b_3 \sqrt{c} \tag{8}$$
$$\text{with } c(x,0) = c_{\text{ref}}, \qquad L_2 < x < L, \; t > 0.$$

Symmetry and continuity of the concentation are also preserved at the grid in the center of the positive electrode by

$$\frac{\partial c}{\partial x}(L,t) = 0, \;\; t > 0. \tag{9}$$

Note that the coefficients are defined in terms of chemical and material properties of the VRLA battery under discharge. The effective diffusion rate includes the reference diffusion coefficient D, and the porosity ε. The reaction rate coefficient is an expansion of the standard Butler–Volmer equation [12]

$$b_j = \frac{A_j^S i_j^0 K_j}{\varepsilon_j \sqrt{c^0}} \cdot \left(\exp\left\{ \frac{\alpha_j F \eta_j}{RT} \right\} - \exp\left\{ \frac{(\alpha_j - 2) F \eta_j}{RT} \right\} \right)$$
$$j = 1, 3$$

where $b_2 = 0$ due to the nonreactive separator material, A^S is the active surface area, i^0 is the exchange current density, c^0 is the reference concentration, α is the anodic apparent transfer coefficient, η is the surface overpotential, R is the universal gas constant, T is the temperature, and K is the equivalent molarity to charge constant, which is defined in the negative electrode, separator, and positive electrode regions represented by $[-, \mathrm{SEP}, +]$ as

$$K = \left[-\frac{2t_+ - 1}{2F}, \; 0, \; \frac{2t_+ - 3}{2F} \right]$$

where F is Faraday's constant, and t_+ is the transference number. Note that each parameter is piecewise constant in relation to the three regions.

C. Voltage Model

Battery voltage is a combination of equilibrium potential and voltage drops caused by cell resistance and generated current, for each of the six battery cells that are connected in series for the batteries tested. Focusing on a battery cell individually, the equilibrium potential is modeled by the Nernst equation [23], [24]. Following our simplifying assumptions, the Nernst equation is derived from first principles using the ideal gas law to quantify the vapor pressure above the solution, Raoult's law to relate to the activity of this nonideal liquid, reversible isothermic work to transfer electrolyte ions across the interfaces, and finally obtaining the equilibrium voltage through the change in Gibb's free energy of the chemical reaction

$$\mathrm{Pb} + \mathrm{PbO_2} + 2\mathrm{H^+} + 2\mathrm{HSO_4^-} \overset{\text{discharge}}{\rightleftharpoons} \mathrm{PbSO_4} + 2\mathrm{H_2O}.$$

Further assuming that this strong acid quickly and equally dissociates, we equate the activities of the sulfuric acid ions and quantify this activity by the activity coefficient and minimum acid concentration. Also, since the electrolyte is largely water, its change in energy is ignored, along with those of the electrode materials.

Thus, by combining the equilibrium potential from the Nernst equation with voltage drops associated with the generated current and cell resistance, the battery voltage is computed for six battery cells in series

$$V = 6 \left((U_3^0 - \eta_3) - (U_1^0 - \eta_1) + \frac{RT}{F} \ln\left(f c_{\min} \right) - N^{\mathrm{cell}} i^{\mathrm{cell}} r \right) \tag{10}$$

where U_1^0, U_3^0 are the two half-electrode potentials, η_1, η_3 are the two overpotentials reducing their respective electrode potentials, f is the mean molar activity coefficient, $c_{\min}$ is the minimum concentration at that time step, N^{cell} is the number of cell pairs in a cell, i^{cell} is the current in each cell pair, and r is the bulk cell resistance.

III. Numerical Method

In order to overcome the complexity caused by the parameter discontinuities and the nonlinearity of the problem, we implement an operator splitting method to solve the governing system (1)–(9). The general form of the governing equations

$$\frac{\partial c}{\partial t} = \frac{D}{\sqrt{\varepsilon_j}} \frac{\partial^2 c}{\partial x^2} - b_j \sqrt{c}, \quad t > 0$$

is split into a reaction step

$$\frac{\partial c}{\partial t} = -b_j \sqrt{c}, \quad t > 0 \tag{11}$$

which happens to be spatially independent, and a diffusion step

$$\frac{\partial c}{\partial t} = \frac{D}{\sqrt{\varepsilon_j}} \frac{\partial^2 c}{\partial x^2} \quad t > 0 \tag{12}$$

which is linear. Simplified as such, we solve the reaction step exactly

$$\mathbf{R}(c_i^n, \Delta t) = \left(-\frac{b_j \Delta t}{2} + \sqrt{c_i^n} \right)^2$$

and solve the diffusion step with an implicit backsolve

$$\mathbf{B}\mathbf{c}^{n+1} = \mathbf{c}^n \tag{13}$$

where we construct the approximation matrix $\mathbf{B}$ as shown in the Appendix.

The PDE is split by solving a reaction step (11) from time index n to $n+1$ and then a diffusion step (12) from n to $n+1$, reevaluating the same time interval. In linear theory, this type of splitting is first-order accurate in time [25]. Theoretical justification and numerical verification of this accuracy are presented in the Appendix. To solve the diffusion split problem numerically, we discretize and apply the diffusion equation to each region disjointly so that the 1-D cell pair is discretized into $3m$ intervals, with m nodes per region, each centered in an interval so as to avoid computing the concentration at the electrode–separator interfaces. Accordingly, the spatial derivatives of the model (1–9) are approximated in each region independently up to the boundaries using one-sided schemes and ghost points. The regions are then coupled through the substitutions of the boundary conditions at the interfaces.

Refer to Fig. 2 for a diagram of this discretization. Note that in giving each region m nodes, the spatial step sizes differ. If the

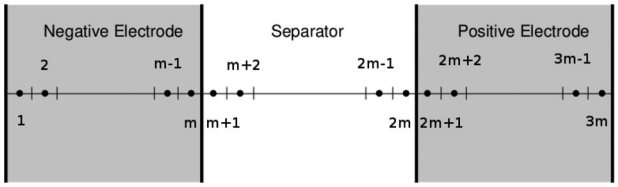

Fig. 2. Discretization of 1-D reduction of a battery cell pair. Note that the nodes m and $2m$ precede their respective interfaces.

separator is thicker than each half-electrode, then this adaptive mesh accesses greater precision in the electrodes, where the nonlinear reaction occurs. In analyzing the method with different step sizes, we utilize $\Delta x = \max\{\Delta x_1, \Delta x_2, \Delta x_3\}$, where Δx_j is the spatial step in region j.

For all inner nodes not neighboring the boundaries or interfaces, the diffusion equation is discretized with $O(\Delta t + \Delta x^2)$ accuracy

$$\begin{aligned}\frac{\partial}{\partial t}c_i^{n+1} - \frac{D}{\sqrt{\varepsilon}}\frac{\partial^2}{\partial x^2}c_i^{n+1} \\ = \frac{c_i^{n+1} - c_i^n}{\Delta t} - \frac{D}{\Delta x^2\sqrt{\varepsilon}}\frac{c_{i-1}^{n+1} - 2c_i^{n+1} + c_{i+1}^{n+1}}{\Delta x^2} \\ + O(\Delta t + \Delta x^2). \end{aligned} \tag{14}$$

For the boundary nodes, the boundary conditions are approximated using the ghost point method, as it matches the second-order spatial accuracy. Note that because the nodes are centered inside each interval the 0-node and the 1-node are centered about the boundary of the negative electrode grid. This is similar for the $3m$ and $(3m+1)$ nodes neighboring the positive grid

$$\begin{aligned}\frac{\partial}{\partial x}c_{1/2}^{n+1} = 0 \rightarrow c_0^{n+1} = c_1^{n+1} + O(\Delta x^2) \\ \frac{\partial}{\partial x}c_{3m+1/2}^{n+1} = 0 \rightarrow c_{m+1}^{n+1} = c_m^{n+1} + O(\Delta x^2). \end{aligned} \tag{15}$$

For nodes neighboring the interfaces, we develop second-order one-sided schemes using the method of undetermined coefficients to reevaluate the spatial diffusion. For example, (16) represents the left-sided scheme at the negative electrode and separator interface

$$\begin{aligned}\frac{\partial^2 c_m^{n+1}}{\partial x^2} \\ = \frac{-\frac{1}{5}c_{m-2}^{n+1} + 2c_{m-1}^{n+1} - 5c_m^{n+1} + \frac{16}{5}c_{m+1/2}^{n+1}}{\Delta x^2} + O(\Delta x^2). \end{aligned} \tag{16}$$

We also develop second-order one-sided schemes to approximate the flux preserving conditions. Equation (17) demonstrates the left-sided scheme at the negative electrode and separator interface, for example

$$\begin{aligned}\frac{\partial}{\partial x}c_{m+1/2^-}^{n+1} \\ = \frac{1}{\Delta x}\left(\frac{1}{3}c_{m-1}^{n+1} - 3c_m^{n+1} + \frac{8}{3}c_{m+1/2}^{n+1}\right) + O(\Delta x^2). \end{aligned} \tag{17}$$

Interface conditions on each side are matched to remove dependence on the interface "nodes" such as $c_{m+1/2}$ in (17).

Combining the results of these substitutions (14, 15, 16, 17) into the diffusion equation (12), we obtain the system of equations $c^n = \mathbf{B}c^{n+1}$ (13), where the $3m \times 3m$ matrix $\mathbf{B}$ is pentadiagonal.

A. Accuracy and Stability Analysis

Method's accuracy is accumulated from the accuracy of each split solution as well as the way the split solutions are recombined. Since the sulfuric acid reaction–diffusion model is a parabolic PDE with infinitely differentiable operators, the split recombination scheme used in Section III provides an $O(\Delta t)$ accuracy for the operator splitting, as theoretically proven and numerically verified by Harwood [26]. Additionally, the spatial diffusion and boundary conditions were discretized with $O\left(\Delta x^2\right)$ accuracy, the reaction split solution was solved exactly, and the diffusion split solution was solved numerical with $O(\Delta t)$ accuracy. Thus, the cumulative accuracy of the numerical solution to the sulfuric acid reaction–diffusion model is first order in time and second order in space.

Since these split solutions are iterated sequentially, stability of the splitting method depends solely on the stability of it's split solutions [25]. The reaction step is solved exactly, and is, hence, unconditionally stable. The diffusion step is solved implicitly by the backward Euler method and is, thus, unconditionally stable [26], [27]. Therefore, the entire numerical solution of the sulfuric acid reaction–diffusion model 1 is unconditionally stable.

Having no stability condition on step sizes, we simply choose the time step as $\Delta t = 100$ ms and divide each region into 20 intervals to obtain spatial step sizes of $\Delta x_1 = 27.3$ μm, $\Delta x_2 = 70.0$ μm, and $\Delta x_3 = 27.3$ μm for the three material regions.

IV. Results

A. Model Parameters

In 2006, batteries designed by CISR (Univ. Idaho, ID) were manufactured and tested at an outside company to conduct discharge tests for measuring voltage. These batteries were composed of six cells, and each cell had 13 negative plates and 12 positive plates. Parameters $c^0, i^{\text{app}}, L, T,$ and η are calculated from measurements taken before testing; $A, i^0, t_+, \varepsilon,$ and f are taken from the literature [14], [23], [24], while the reference diffusion rate D and cell resistance r were optimized within an order of magnitude of listed values [12]*, [24]* to calibrate the simulated voltage to the hand-pasted battery data. Fig. 3 shows the numerical solution of acid concentration model (1)–(9) under discharge with the parameter values listed in Table I.

Compared to a fully implicit solution of the whole system, this decoupled operator splitting resulted in remarkable speedup, as shown in Table II. For each number of total spatial nodes, the runtime of the method's computation, not including variable creation and post-processing, of 2000 simulated seconds with a $\Delta t = .25$ s time step is shown. To calculate speedup of our operator splitting method, we developed a semi-implicit full

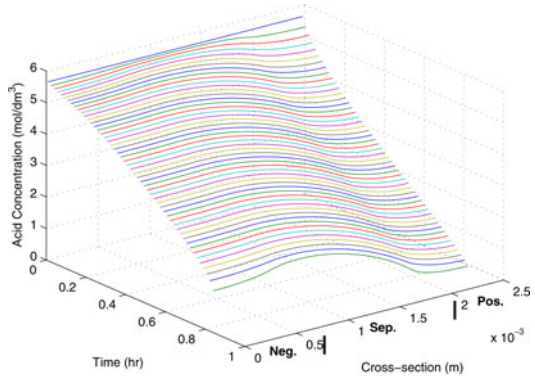

Fig. 3. Numerical solution for acid concentration of model (1)–(9) during discharge at 27 A.

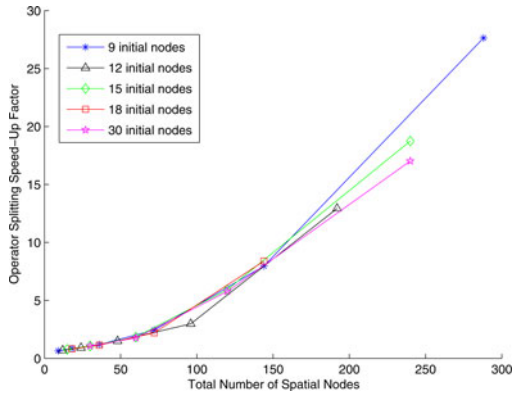

Fig. 4. Computational speedup of our operator splitting method is computed for sequences of spatial mesh refinement using four different initial spatial nodes.

TABLE I
PARAMETER VALUES USED IN NUMERICAL SOLUTION

Symbol	Negative Electrode	Separator	Positive Electrode	Units [Source]
A	74.2	–	74.2	cm^2 [28]
A^S	237	0	2070	m^2/m^3 [14]
c^0	5.65	5.65	5.65	mol/L [28]
D	1.13×10^{-9}	1.13×10^{-9}	1.13×10^{-9}	m^2/s [12]*
f	0.198	0.198	0.198	mol/L [24]
i^{batt}	27	–	27	A [28]
i^0	1040	–	66.6	A/m^2 [14]
L	0.546	1.40	0.546	mm [28]
r	0.080	0.080	0.080	Ω [24]*
T	311	311	311	K [28]
t^+	0.72	–	0.72	– [14]
U^0	-0.360	–	1.81	V [24]
α	1.55	–	1.15	– [14]
ϵ	0.5	0.9	0.45	– [14]

TABLE II
COMPUTATIONAL RUNTIME AND SPEEDUP OF OPERATOR SPLITTING

Number of Total Nodes	Split Run-Time	Full Run-Time	Speed-Up Factor	Acceleration Factor
9	0.65 s	0.43 s	0.65	–
18	0.77 s	0.65 s	0.85	1.30
36	0.99 s	1.19 s	1.20	1.42
72	1.39 s	3.39 s	2.44	2.03
144	1.45 s	11.53 s	7.97	3.26
288	2.38 s	65.64 s	27.63	3.47

method that computes the reaction term from the previous solution while implicitly solving the system. The posted speedup factor is the runtime for this full method divided by the runtime for the given operator splitting method, both solved over the same spatial mesh size. To demonstrate the superlinear nature of this speedup, we further computed an "acceleration" factor, which is the factor by which the speedup has increased from the previous mesh size. Tenno *et al.* [14] used 18 total nodes (six layers per region) in their discretization with time step $\Delta t = .25$ s to obtain as fast as "real-time simulation" runtimes for 6-h and 1-h rate discharges. Assuming their 1-h rate simulation ran for 3600 s at $\Delta t = 0.25$ s, then our split method runtime of 0.77 s shows approximately a 4675 times improvement in computational time due to the model simplifications and operator splitting. The runtime for the split method is longer in comparison to the full method for coarse spatial meshes, as shown for 9 and 18 total nodes in Table II, when updating the matrix for the full method is less costly than the computational overhead of recombining split solutions. Yet, as the spatial mesh is refined, the computational benefits of operator splitting become clear. While Table II demonstrates speedup by repeatedly refining one spatial mesh size, Fig. 4 shows the speedup for refinement sequences of five initial mesh sizes, and it is clear that these sequences of speedup factors overlap to form a superlinear curve. This agrees with the increasing acceleration factors in Table II. These tests were run in MATLAB on a single desktop with a dual core processor.

Unlike other calculated parameters, the overpotential, which maintains its initial value due to a constant discharge current, is defined by the following differential inverse problem:

$$\left(\frac{\partial i}{\partial x}\right)_j = i_j^0 K_j \cdot \left(\exp\left\{\frac{\alpha_j F \eta_j}{RT}\right\} - \exp\left\{\frac{(\alpha_j - 2)F\eta}{RT}\right\}\right)$$

with $i = 0$ at the separator, and $i = i_{\text{app}}$ at the outer boundaries; all parameters are piecewise continuous with respect to each region j. We solve this problem for the overpotential in the two electrodes η_1 and η_3 using a Newton inexact line search [29]

$$\eta_j^{(k+1)} = \eta_j^{(k)} - \frac{E_j(\eta_j^{(k)})}{\frac{\partial}{\partial \eta} E_j(\eta_j^{(k)})}, \quad j = 1, 3$$

bounded between -1 V and 1 V, where these iterative methods started with initial guesses of -1 and 1 for $j = 1$ and -1, respectively, converge linearly to the respective overpotential, and stops when $|\eta_j^{(k+1)} - \eta_j^{(k)}| < \text{tol}$ for a small tolerance: tol $= 0.1$. The error functions $E_j(\eta_j^{(k)})$ are defined for each electrode as

$$E_1(\eta_1) = L_1 \left(\frac{\partial i}{\partial x}\right)_1 - i^{\text{app}}$$

$$E_3(\eta_3) = L_3 \left(\frac{\partial i}{\partial x}\right)_3 + i^{\text{app}}.$$

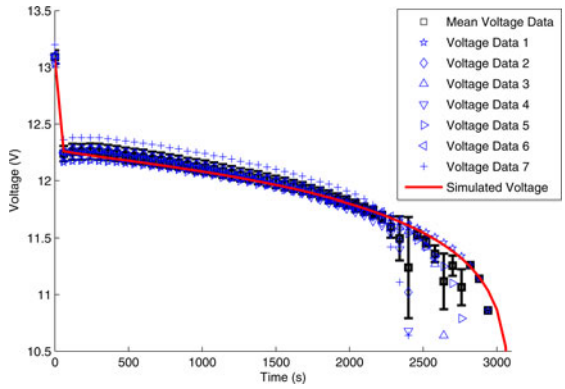

Fig. 5. Comparison of simulated voltage against 27 A discharge measurements of one batch of seven uniformly designed batteries.

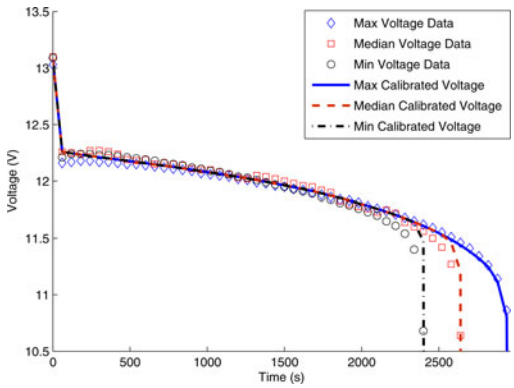

Fig. 6. Comparison of simulated and measured battery voltages at 27 A discharge current for two data strands of various charge capacities. The maximum allowable utilization is calibrated to simulate the variability.

Data collected for 27 A discharges are compared as a whole to the simulated voltage in Fig. 5 to demonstrate data variability. Although the simulated voltage for a fully charged battery qualitatively fits this batch of data, the simulated voltage does not remain within the error bars, which mark one standard deviation about the mean. It is clear that the high variability at the end of discharge represents more than random errors. Thus, we calibrate our model by adjusting the maximum allowable utilization to account for batteries that were not fully charged on this first discharge test. As shown in Fig. 6, we optimize the maximum allowable utilizations to simulate the maximum, median, and minimum batteries chosen from the given batch. Computing the difference between these three values, we can also hypothesize how much of each battery was unformed at the beginning of discharge, assuming that the longest living battery was fully charged.

Comparing the simulation results to this batch of uniformly designed batteries requires further information about the variability in the data, as random variation is inadequate to account for such wide variation in discharge end times. The batteries tested were newly formed and had not yet been cycled up for uniform fullness of charge; each battery was only discharged once [28]. Besides random variation, we assume that the only difference between the discharges is the fullness of charge represented by the critical volume fraction u_j^{CVF}, which is also the maximum allowable utilization for electrode $j = 1, 3$.

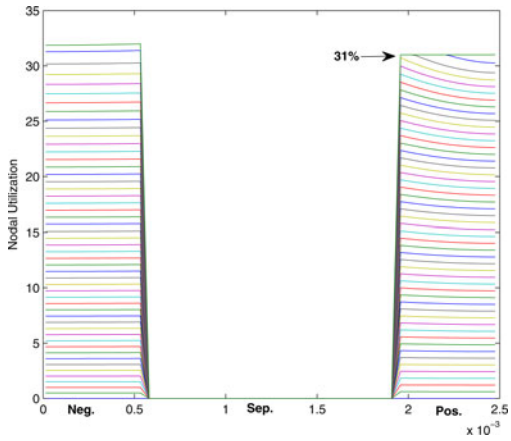

Fig. 7. Utilization profile for the maximum calibrated voltage. Notice that the positive utilization equals the maximum allowable utilization of 31%.

Due to conductive pathway constraints [30], nodes cannot be utilized beyond a critical volume fraction, which has been experimentally and theoretically approximated between 55% and 65% in the positive electrode [22], [31]. Since this is more limiting in the positive electrode, we focus our calibration on the maximum allowable utilization for those nodes. Cells not fully charged, however, have less capacity and, thus, a lower maximum allowable utilization than the electrodes' critical volume fraction [5]. When a nodes' utilization reaches this maximum allowable utilization, that node is shut off, shifting the weight of the discharge to neighboring nodes. The utilization at each node u is summed over time as

$$u = \sum \frac{\Delta V_j \Delta c}{\kappa_j W_j K_j}$$

where $\Delta V_j = \varepsilon_j A_j \Delta x_j$ is the nodal volume of acid in the jth region, $\Delta c = |c^n - c_R^n|$ is the absolute change in acid concentration due to each reaction step, and K_j is the molar-to-charge ratio per region j. To reduce our simulated voltage to match the three batteries chosen to represent the test batch, we calibrate our maximum allowable nodal utilizations in the positive plate from 31.0% for the maximum life battery to 27.5% for the median and 25.0% for the minimum life battery. Fig. 6 provides a comparison between the calibrated simulated voltages to these three battery discharges representing the extreme and median life of the seven batteries of the batch tested. These optimal calibrations to the data produce standard errors of 0.0260, 0.0963, and 0.1326 V between the simulated and measured voltages for the maximum-, median-, and minimum-life battery representatives.

Due to the simplicity of our model, these utilization caps are in fact the utilizations of the whole positive electrode, as shown in Fig. 7. Thus, it is inconclusive to compare them to the critical volume fraction approximated previously. Yet, in computing the relative differences between these utilizations, we can still compute the variation in fullness of charge and approximate how fully charged each battery was when initially discharged. Assuming that the maximum battery was fully charged, the 3.5% difference suggests that the median battery was 96.5% fully charged, and the further 6.0% difference suggests that the minimum battery was 93.0% fully charged when first tested. As representative of this batch of batteries, these three indicate that

there was only a 6.0% variation in fullness of charge, assuming the maximum battery was indeed fully charged.

V. Summary and Conclusion

Our reduction to the simplified sulfuric acid model (1)–(9) produced results as expected. The operator splitting method used to separate this PDE into linear and solvable nonlinear pieces produced a smooth reaction–diffusion of the electrolyte. The profile of the acid concentration in Fig. 3 smoothly decreases through reaction in the electrodes and diffusion from the separator into each electrode. The speedup associated with using the operator splitting method in favor of a fully implicit solution is quite remarkable, especially for finer meshes (more than 18 total nodes). This computational speedup is superlinear, as the acceleration in the speedup factor remains above 1, and is in fact better than exponential speedup as this acceleration also remains above 1 and is strictly increasing. Supported by these results, this decoupled operator splitting should be particularly effective for large-scale systems.

A model for voltage was derived via the Nernst equation (10) from the simulated concentration, and is used to compare with measured data. This data, however, are not uniform, as demonstrated in Fig. 5, though the batteries were manufactured to fit the same design. We developed a dependence on maximum allowable utilization to model this variability in the data. In calibrating our simulation to fit the data and in the process we were able to approximate the percentage of formation of each battery before they are cycled up to a more uniform charge formation. This percent formulation capacity relates the life of the battery to the conductivity of the formation of the battery electrodes.

Appendix

Seeking the system of equations that define the diffusion split problem across the discretized composite material, we combine the substitutions of (14), (15), (16), and (17) into the diffusion equation (12), and using the simplifying variables

$$\lambda_j = \frac{D\Delta t}{\sqrt{\varepsilon_j}\Delta x^2}$$

$$\delta_{jk} = \frac{\Delta x_k \sqrt{\varepsilon_k}}{\Delta x_j \sqrt{\varepsilon_j} + \Delta x_k \sqrt{\varepsilon_k}}$$

we obtain the following equations in the negative electrode ($-$), separator (SEP), and positive electrode ($+$) material regions:

$$
-\begin{cases}
c_1^n = (1+\lambda_1)\, c_1^{n+1} - \lambda_1 c_2^{n+1} \\
c_i^n = -\lambda_1 c_{i-1}^{n+1} + (1+2\lambda_1)\, c_i^{n+1} - \lambda_1 c_{i+1}^{n+1} \\
\qquad \boxed{i = 2 : m-1} \\
c_m^n = \dfrac{\lambda_1}{5} c_{m-2}^{n+1} - \left(2 - \dfrac{2\delta_{12}}{5}\right)\lambda_1 c_{m-1}^{n+1} \\
\qquad + \left(1 + \left(5 - \dfrac{18\delta_{12}}{5}\right)\lambda_1\right) c_m^{n+1} \\
\qquad - \dfrac{18\delta_{21}\lambda_1}{5} c_{m+1}^{n+1} + \dfrac{2\delta_{21}\lambda_1}{5} c_{m+2}^{n+1}
\end{cases}
$$

$$
\mathrm{SEP}\begin{cases}
c_{m+1}^n = \dfrac{2\delta_{12}\lambda_2}{5} c_{m-1}^{n+1} - \dfrac{18\delta_{12}\lambda_2}{5} c_m^{n+1} \\
\qquad + \left(1 + \left(5 - \dfrac{18\delta_{21}}{5}\right)\lambda_2\right) c_{m+1}^{n+1} \\
\qquad - \left(2 - \dfrac{2\delta_{21}}{5}\right)\lambda_2 c_{m+2}^{n+1} + \dfrac{\lambda_2}{5} c_{m+3}^{n+1} \\
c_i^n = -\lambda_2 c_{i-1}^{n+1} + (1+2\lambda_2)\, c_i^{n+1} - \lambda_2 c_{i+1}^{n+1} \\
\qquad \boxed{i = m+2 : 2m-1} \\
c_{2m}^n = \dfrac{\lambda_2}{5} c_{2m-2}^{n+1} - \left(2 - \dfrac{2\delta_{23}}{5}\right)\lambda_2 c_{2m-1}^{n+1} \\
\qquad + \left(1 + \left(5 - \dfrac{18\delta_{23}}{5}\right)\lambda_2\right) c_{2m}^{n+1} \\
\qquad - \dfrac{18\delta_{32}\lambda_2}{5} c_{2m+1}^{n+1} + \dfrac{2\delta_{32}\lambda_2}{5} c_{2m+2}^{n+1}
\end{cases}
$$

$$
+\begin{cases}
c_{2m+1}^n = \dfrac{2\delta_{23}\lambda_3}{5} c_{2m-1}^{n+1} - \dfrac{18\delta_{23}\lambda_3}{5} c_{2m}^{n+1} \\
\qquad + \left(1 + \left(5 - \dfrac{18\delta_{32}}{5}\right)\lambda_3\right) c_{2m+1}^{n+1} \\
\qquad - \left(2 - \dfrac{2\delta_{32}}{5}\right)\lambda_3 c_{2m+2}^{n+1} + \dfrac{\lambda_3}{5} c_{2m+3}^{n+1} \\
c_i^n = -\lambda_3 c_{i-1}^{n+1} + (1+2\lambda_3)\, c_i^{n+1} - \lambda_2 c_{i+1}^{n+1} \\
\qquad \boxed{i = 2m+2 : 3m-1} \\
c_{3m}^n = -\lambda_3 c_{3m-1}^{n+1} + (1+\lambda_3)\, c_{3m}^{n+1}.
\end{cases}
$$

These equations represent the system $c^n = \mathbf{B}c^{n+1}$ (13), where the $3m \times 3m$ matrix $\mathbf{B}$ for the diffusion step is pentadiagonal. Notice, however, that $\mathbf{B}$ has only four rows with five nonzero entries; the rest have three which is standard to a tridiagonal matrix.

Acknowledgment

For the cooperation and technical expertise in the chemical, material, and structural dynamics of VRLA batteries, the authors would like to thank the researchers at the CISR, University of Idaho, especially T. Bean, S. Zhang, and J. Canning.

References

[1] U. S. DOE, "Weekly United States Spot Price F.O.B. Weighted by Estimated Import Volume," *Energy Information Administration*, Sep. 22, 2010.

[2] U. S. DOE, "Monthly U.S. Total Gasoline All Sales/Deliveries by Prime Supplier," *Energy Information Administration*, Sep. 23, 2010.

[3] U. S. DOE, "Weekly U.S. Petroleum Products Product Supplied," *Energy Information Administration*, Sep. 23, 2010.

[4] P. W. Appel, D. B. Edwards, and T. Stalick, "Modeling the effects of electrolyte diffusion and paste conductivity on lead-acid battery performance," *J. Power Sources*, vol. 46, pp. 49–60, 1987.

[5] S. Zhang, "Investigating paste additives to improve the specific energy performance of a lead acid battery," Ph.D. dissertation, Dept. Mech. Eng., Univ. Idaho, Moscow, 2005.

[6] D. B. Edwards and V. Srikanth, "Evaluation of hollow, glass microspheres used as an additive in positive, lead acid battery paste," *J. Power Sources*, vol. 34, no. 3, pp. 217–232, 1991.

[7] D. B. Edwards, P. W. Appel, and B. Hammond, "Evaluation of hollow, glass microspheres used as an additive in negative, lead acid battery paste," *J. Power Sources*, vol. 38, pp. 287–294, 1992.
[8] R. L. Cantrell, D. B. Edwards, and P. S. Gill, "Predicting lead-acid battery electrode performance using finite difference equations," *J. Power Sources*, vol. 73, no. 2, pp. 204–216, 1998.
[9] W. Stein, "Die Vorgänge in den Poren von Masseplatten bei der Entladung des Bleisammlers mit großen Stromdichten," *Naturwissenschaften*, vol. 45, pp. 459–460, 1958.
[10] J. Euler, "Porendimensionen und Oberflächenkapazität von Braunstein," *Electrochim. Acta*, vol. 4, no. 1, pp. 27–41, 1961.
[11] J. Newman and W. H. Tiedemann, "Porous-electrode theory with battery applications," *AIChE J.*, vol. 21, pp. 25–41, 1975.
[12] H. Gu, T. V. Nguyen, and R. E. White, "A mathematical model of a lead-acid cell," *J. Electrochem. Soc.*, vol. 134, no. 12, pp. 2953–2960, 1987.
[13] Z. M. Salameh, M. A. Casacca, and W. A. Lynch, "A mathematical model for lead-acid batteries," *IEEE Trans. Energy Convers.*, vol. 7, no. 1, pp. 93–98, Mar. 1992.
[14] A. Tenno, R. Tenno, and T. Suntio, "Charge-discharge behaviour of VRLA batteries," *J. Power Sources*, vol. 103, pp. 42–53, 2001.
[15] C. J. Zhan, X. G. Wu, S. Kromlidis, and V. K. Ramachandaramurthy, "Two electrical models of the lead-acid battery used in a dynamic voltage restorer," *IEE Proc. Gener., Transmiss. Distrib.*, vol. 150, no. 2, pp. 175–182, 2003.
[16] P. M. Hunter and A. H. Anbuky, "VRLA battery virtual reference electrode: Battery float charge analysis," *IEEE Trans. Energy Convers.*, vol. 23, no. 3, pp. 879–886, Sep. 2008.
[17] C. R. Gould, C. M. Bingham, D. A. Stone, and P. Bentley, "New battery model and state-of-health determination through subspace parameter estimation and state-observer techniques," *IEEE Trans. Veh. Technol.*, vol. 58, no. 8, pp. 3905–3916, Oct. 2009.
[18] P. W. Appel, "Modeling and verifying the performance of lead-acid battery cell with paste additives," Ph.D. dissertation, Dept. Mech. Eng., Univ. Idaho, Moscow, 1994.
[19] P. S. Gill, "A finite difference model for simulating the discharge behavior of the positive electrode in lead-acid cells," M.S. thesis, Dept. Mech. Eng., Univ. Idaho, Moscow, 1995.
[20] R. L. Cantrell, "Modeling and designing a high performance lead-acid battery for hybrid electrical vehicle," M.S. thesis, Dept. Mech. Eng., Univ. Idaho, Moscow, 1996.
[21] D. B. Edwards and S. Zhang, "A three-dimensional conductivity model for electrodes in lead acid batteries," *J. Power Sources*, vol. 158, pp. 927–931, 2006.
[22] S. Zhang, T. Bean, and D. B. Edwards, "Examination of different lattice structures in porous electrodes using a three-dimensional conductivity model," *J. Power Sources*, vol. 195, pp. 883–889, 2009.
[23] D. Berndt, *Maintenance-Free Batteries*: 3rd ed. Baldock, U.K.: Research Studies Press, Ltd, 2003.
[24] T. R. Crompton, *Battery Reference Book*: 2nd ed. Oxford, England: Butterworth–Heinemann, 1995.
[25] G. Strang, "On the construction and comparison of difference schemes," *SIAM J. Numer. Anal.*, vol. 5, pp. 506–517, 1968.
[26] R. C. Harwood, "Operator splitting method and applications for semilinear parabolic partial differential equations," Ph.D. dissertation, Dept. Math., Washington State Univ., Pullman, 2011.
[27] R. Burden and J. D. Faires, *Numerical Analysis*, 5th ed. Boston, MA: PWS-Kent, 1993.
[28] A. Paryani, "Concorde battery test for HE HMMWV," Concorde Battery Corp., West Covina, CA, Tech. Rep., 2007.
[29] J. Nocedal and S. J. Wright, *Numerical Optimization*, 2nd ed. New York: Spring-Verlag, 2006.
[30] D. B. Edwards and S. Zhang, "Influence of different aspect ratio additives on the performance of lead-acid batteries," *J. Power Sources*, vol. 135, pp. 297–303, 2004.
[31] S. Zhang and D. B. Edwards, "Three-dimensional conductivity model for porous electrodes in lead acid batteries," *J. Power Sources*, vol. 172, pp. 957–996, 2007.

Richard Corban Harwood received the B.S. degree from Whitworth University, Spokane, WA, in 2006, and the M.S. and Ph.D. degrees in mathematics from Washington State University, Pullman, in 2008 and 2011, respectively.

He is currently an Assistant Professor of Mathematics at George Fox University, Newberg, OR. His research interests include modeling reaction–diffusion phenomena and developing fast numerical methods, specifically operator splitting methods, for semilinear partial differential equations.

Valipuram S. Manoranjan received the B.S. degree from the University of Sri Lanka, Sri Lanka, in 1977, and the Ph.D. degree from the University of Dundee, Scotland, in 1982.

He was a Research Fellow at the University of Oxford, England, and a Faculty Member in the Department of Chemical and Process Engineering, University of Surrey, England, prior to joining Washington State University, Pullman, in 1989, where he is currently a Professor of Mathematics. His research interests include mathematical and computational modeling of nonlinear systems that arise in engineering and life sciences—in particular, constructing simple, efficient, and accurate numerical schemes for nonlinear partial differential equations.

Dean B. Edwards received the B.S. degree from the Illinois Institute of Technology, Chicago, in 1972, and the M.S. and Ph.D. degrees from the California Institute of Technology, Pasadena, in 1973 and 1977, respectively.

From 1977 to 1986, he was at the Jet Propulsion Laboratory, Pasadena, CA, before moving to the University of Idaho, Moscow, in 1986, where he is currently a Professor of Chemical and Materials Engineering. His research is focused on developing high-power, cost-effective batteries for use in plugin, hybrid electric vehicles.